Electron and Hole Trapping in Ce^{3+}- and Pr^{3+}-Doped Lutetium Pyrosilicate Scintillator Crystals Studied by Electron Paramagnetic Resonance

V. Laguta,[1,*] M. Buryi,[1] Y. Wu,[2] G. Ren,[2] and M. Nikl[1]

[1] *Institute of Physics of the Czech Academy of Sciences, Cukrovarnicka 10/112, Prague, Czech Republic*

[2] *Shanghai Institute of Ceramics, Chinese Academy of sciences, 585 He-shuo Road, Shanghai 201899, P.R. China*

(Received 2 December 2019; revised manuscript received 30 January 2020; accepted 7 April 2020; published 23 April 2020)

Electron and hole trapping is studied in the Ce^{3+}- and Pr^{3+}-doped $Lu_2Si_2O_7$ scintillation single crystals (LPS:Ce and LPS:Pr) by electron paramagnetic resonance (EPR). Detailed EPR measurements of the x-ray irradiated LPS crystals reveal that holes generated by irradiation are predominantly trapped at oxygen lattice ions creating O^- centers. The same x-ray irradiation creates also electron-type centers, which are attributed to Lu^{2+} ions, where the trapped electron at the Lu lattice ion is stabilized by a nearby defect, such as the oxygen vacancy and Ir^{3+} impurity ion. Both the hole and electron centers can be thus considered as a bound small polaron, which makes the charge trapping in a scintillation mechanism quite competitive. The hole O^- and electron Lu^{2+} centers show thermal stability well above room temperature. Thermal decays of their concentrations correlate well with the appearance of the thermally stimulated luminescence glow peaks at 470–550 K. The presence of the same intrinsic traps in the Ce- and Pr-doped LPS crystals suggests that the difference in the light yield of these crystals is an intrinsic property of the Ce^{3+} and Pr^{3+} activator centers in the LPS lattice. An origin of charge traps in this pyrosilicate structure and their role in the scintillation mechanism is compared with the results previously described in the literature on orthosilicates.

DOI: 10.1103/PhysRevApplied.13.044060

I. INTRODUCTION

Along with the Ce-doped lutetium oxyorthosilicate Lu_2SiO_5 (LSO:Ce), the Ce- and Pr-doped lutetium pyrosilicate $Lu_2Si_2O_7$ (LPS) crystals are very promising candidates for detection of γ rays in positron-emission tomography (PET) and high-energy calorimetry [1]. LSO:Ce and LYSO:Ce crystals are currently used in scintillation detectors in PET scanners and various codoping schemes have been reported in the last decade to further improve their performance [2–5]. In this respect, LPS:Ce shows even better scintillation properties. In particular, having approximately the same light yield (LY), energy resolution, and decay time as reported in LSO:Ce, it is free from an intense afterglow [6,7] usually present in LSO:Ce. However, the experimentally measured LY of 26 000–30 000 ph/MeV is still much smaller than the theoretical maximum of about 55 000–60 000 ph/MeV [2,8]. The difference between theoretical and experimental light outputs could be linked either to material defects that could trap electrons or holes created during irradiation, or to efficiency of the electron-hole recombination at the Ce^{3+} or Pr^{3+} centers. Several peaks observed around 460 and 550 K in the thermoluminescence (TL) curve [6,7,9] confirm the existence of traps in the material.

As emphasized in Ref. [10], a serious disadvantage of this crystal is a lack of light-yield reproducibility for crystals grown by the Czochralski method. It was suggested [10] that some impurities or defect states (traps) are responsible for the light-yield quenching since Ce^{3+} in this lattice does not show any significant intrinsic luminescence quenching around room temperature. Electron paramagnetic resonance (EPR) study has shown that Ir^{3+} ions incorporated in the crystal from the Ir crucible could be responsible for the LY quenching [10]. Annealing treatments under different temperatures and different atmospheres suggest a significant influence of oxygen vacancies on the light output as well [7].

A more complicated situation occurs in the Pr^{3+}-doped LPS. As a rule, the high-energy-shifted $5d$-$4f$ transition of Pr^{3+} provides a faster response compared to that of Ce^{3+}. Therefore, LPS:Pr also attracted attention as a prospective fast scintillation material. However, its LY is much lower, with respect to that of LPS:Ce [11]. It was explained as being due to the intense slow $4f$-$4f$ emission resulting from an efficient energy transfer from the self-trapped excitons to $4f$ states of Pr^{3+} [11,12]. Later, the radioluminescence (RL) measurement of the LPS:Pr powder prepared by the sol-gel method does not show any

*laguta@fzu.cz

significant contribution of the 4*f* -4*f* emission [13]. Furthermore, some of the Czochralski-grown LPS:Pr crystals manifested the radioluminescence amplitude of the 5*d*-4*f* emission of Pr^{3+} comparable with that of the Ce^{3+}-doped crystals [14]. More detailed study of this phenomenon [15] showed that the RL efficiency increase in the LPS:Pr crystals is due to progressive filling of deep traps responsible for the TL peaks at 460 and 515 K. During irradiation these traps compete with Pr^{3+} ions for the free charge-carrier capture. After filling of the traps the RL increases up by a factor of 14. Because the actual origin of a trap cannot be determined by TL itself, it is speculated that the traps revealed in LPS are intrinsic, and most probably due to oxygen vacancies.

All the facts mentioned demonstrate that the scintillation properties of LPS are quite sensitive to defects created during the crystal growth process. Their origin must be determined in order to further improve scintillation efficiency of LPS crystals. Since the expected defects are intrinsic, their local structure and mechanism of creation are of interest for the chemistry of materials as well.

Charge traps in a scintillating material can usually be monitored by measurements of TL glow peaks after the material is exposed to ionizing irradiation [16]. However, this method cannot determine an actual nature of the trapping center. In this respect, in addition to optical characterization, the advanced EPR methods can provide a microscopic insight into the defect creation and its structure. In particular, EPR allows accompanying electron and hole localized states affecting the efficiency and time characteristics of the scintillation mechanism in the Ce- or Pr-doped scintillation crystals to be distinguished.

In this paper we present the results of a detailed EPR study of the Ce- and Pr-doped LPS crystals grown by the Czochralski method. It is found that, independently of an activator ion type, the same trapping centers are presented in both crystals: holes generated by irradiation are trapped at the oxygen lattice ions and electrons are trapped at the lutetium ions. The trapped holes and electrons are stabilized at the lattice ions by a nearby defect. Obtained data suggest that these intrinsic traps in LPS are polaron-type states. Such a character explains their highly competitive role in the scintillation process.

II. EXPERIMENTAL METHODS

The crystals are grown from the melt by the Czochralski method in atmosphere of highly pure nitrogen by using iridium crucibles [7]. The initial praseodymium and cerium concentrations in the melt are 0.5 and 0.3 at %, respectively, with respect to the total rare-earth sites. It is worth mentioning that the same crystals have already been characterized by TL and other optical measurements [7,9].

LPS crystallizes in the monoclinic structure in the space group $C2/m$ [17]. This lattice exhibits a single crystallographic site for Lu^{3+} ions with six oxygen neighbors forming a distorted octahedron with the C_2 point symmetry. For EPR measurements, crystals are cut in three orthogonal planes (a^*b), (bc), and (a^*c). The axis a^* is deflected from the crystallographic axis a by an angle of 12° in order to satisfy the orthogonality between crystal planes that is necessary for determination of g factors from EPR spectra.

EPR measurements are performed in the X band (9.4 GHz) with a commercial Bruker EMX spectrometer at temperatures 10–100 K. An x-ray tube operating at a voltage and current of 55 kV and 30 mA, respectively, with Co anode (ISO-DEBYEFLEX 3003 Seifert Gmbh.) is used as an x-ray source. The irradiation dose is about 1 kGy.

III. RESULTS AND DISCUSSION

A. EPR spectra in x-ray-irradiated crystals

As-grown LPS crystals, besides the Ce^{3+} EPR spectra (Pr^{3+} EPR transitions are not visible in the X band), also contain the spectra of many other rare-earth ions, such as Yb^{3+}, Er^{3+}, Dy^{3+}. Characteristics of these paramagnetic impurity ions will be the subject of a separate publication. In the present study we are interested in the intrinsic centers related to the trapped hole and electron localized states. As an example, Fig. 1 shows the EPR spectrum measured in LPS:Pr before (a) and after (b) x-ray irradiation at room temperature. Before irradiation, there is only one spectrum (designated as Lu1) related to electron traps with well-resolved hyperfine (HF) structure. As shown below, this

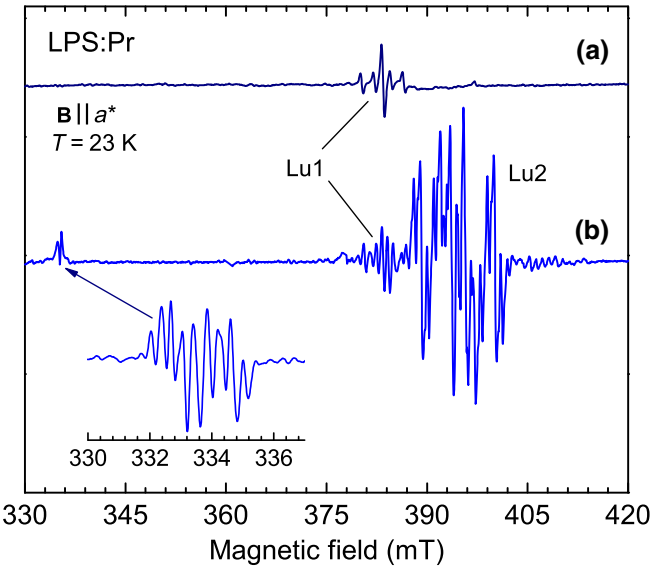

FIG. 1. EPR spectrum before (a) and after (b) x-ray irradiation of LPS:Pr crystal measured at 23 K. Inset shows a spectrum of the hole-trapped center recorded at 100 K, when the spectrum is not distorted by spin-lattice relaxation effects as at 23 K.

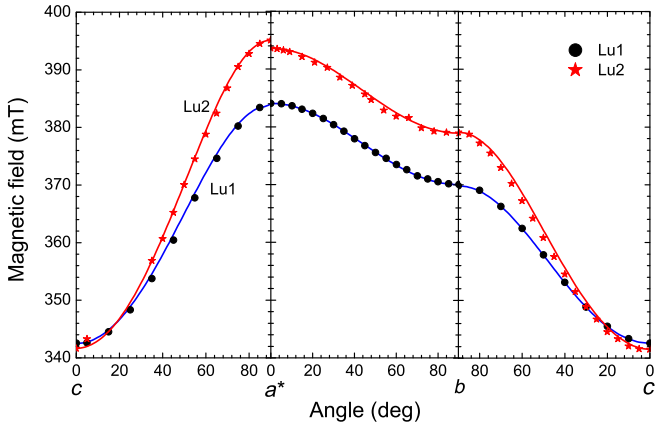

FIG. 2. Angular dependence of the Lu1 and Lu2 resonance fields (center of gravity of their HF structure) measured in three orthogonal planes.

HF structure originates from the interaction of an electron spin with the nuclear spin of ^{175}Lu isotope (nuclear spin $I = 7/2$, 100% natural abundance). After x-ray irradiation at room temperature, two new spectra appear: one spectrum at magnetic fields of 390–400 mT (designated as the trapped electron Lu2 center), and the second one at 332–335 mT. Both spectra show a complex HF structure. The spectrum at lower magnetic fields is assigned to a hole trapped at an oxygen ion, i.e., to the O^- center (see, Sec. III A 2).

1. Trapped electron centers

Angular dependencies of resonance fields (center of gravity of the HF structure) of the Lu1 and Lu2 spectra manifest very similar behavior (Fig. 2). For the Lu1 center they are fitted by the following g factors: $g_1 = 1.746(1)$, $g_2 = 1.813(1)$, $g_3 = 1.957(1)$, where the three principal axes (1, 2, and 3) coincide with the crystallographic a^*, b, and c axes. The obtained g factors are typical of d^1 ions [18].

In order to clarify the origin of both these centers, we first analyze the HF structure of the Lu1 center. Its HF structure consists of eight equidistant components at the magnetic field direction along the c crystal axis (Fig. 3), suggesting that it originates from an isotope with the nuclear spin 7/2 and abundance around 100%. However, as the magnetic field deviates from the c axis, the HF structure becomes unusually complex suggesting that there is a strong contribution of the nuclear quadrupole interaction. It is confirmed by simulation of the HF structure using the following spin Hamiltonian:

$$H = \mu_B \mathbf{BgS} + \mu_n \mathbf{B} g_n \mathbf{I} + \mathbf{SAI} + \frac{\nu_Q}{2}\left[I_z^2 - \frac{1}{3}I(I+1)\right], \quad (1)$$

where $\nu_Q = [3e^2qQ/h2I(2I-1)]$ is the quadrupole frequency. Here, μ_B and μ_n are the Bohr and nuclear magnetons, respectively; **B** is the magnetic field vector, g_n is the nuclear g factor, **A** is the HF tensor, and I_z is a component of the nuclear spin along the main axis of an electric field gradient (EFG), which is assumed to be aligned along the c crystal axis. This assumption is supported by the fact that at the c crystal direction the HF structure is not influenced by quadrupole effects. Because forbidden transitions are dominant in the HF structure at the majority of magnetic field directions, the spin Hamiltonian (1) is solved numerically to provide the correct calculation of resonance fields and transition probabilities in electron and

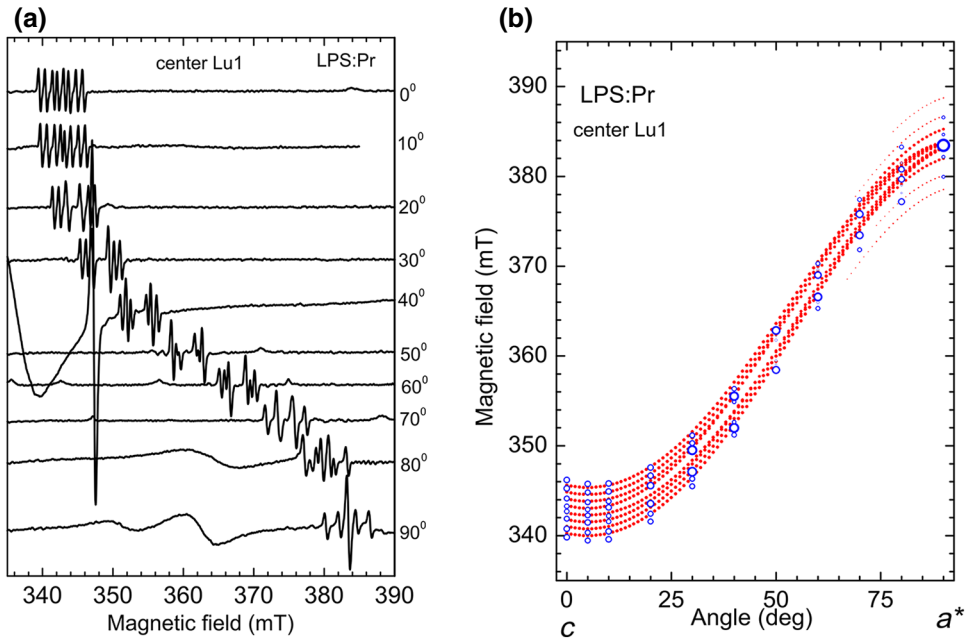

FIG. 3. (a) Angular variation of the Lu1 spectrum in ca^* plane and (b) corresponding numerical fit of the HF lines position. In (b), red dots are calculated resonance fields with the step of 1 deg., blue circles are experimental fields taken from the spectra in (a). Size of the circles and dots is proportional to intensity of spectral component.

nuclear spin systems [19]. The following HF parameters are obtained from the simulation: $A = 7.0 \times 10^{-4}$ cm^{-1} (or 21 MHz), $\nu_Q \approx 100$ MHz, i.e., $\nu_Q \gg A$. The HF constant is nearly isotropic; quadrupole transitions are seen in the HF structure at angles close to the a*-axis direction as weak satellites [Fig. 3(b)]. The calculated angular dependence of the HF components including their intensities adequately describe all characteristic features of the measured ones [Fig. 3(b)]. In particular, eight HF lines grouped into two structures separated by sufficiently large distance of about 3.5 mT at angles between $20 - 70^0$.

Taking into account the g-factor values, nuclear spin, and very large quadrupole frequency for the Lu1 center, the most probable candidate for paramagnetic ion responsible is Lu^{2+}, which has the $5d^1$ outer electronic shell, ^{175}Lu isotope with nuclear spin 7/2, natural abundance 97.4%, and huge quadrupole moment $Q = 349$ fm^2. Among other nd^1 ions, only Ta^{4+} has a suitable isotope with comparable quadrupole moment. Because such a specific HF structure is also observed for other x-ray-created paramagnetic defects in our crystals (Lu2, O^-), we prefer a model with the Lu ion, which is the host lattice cation. More arguments in favor of the Lu^{2+}-related center are given below.

The g factors of the Lu2 center are close to those of the Lu1 center: $g_1 = 1.700(1)$, $g_2 = 1.770(1)$, $g_3 = 1.962(1)$. Within the g-factor determination error they coincide with the g factors of the Ir-related center described in Ref. [10], where it appeared also after x-ray irradiation. It is assigned to the Ir^{4+} ion in a low-spin state of this ion. In our opinion, the similarities in the symmetry and g-factor values of both the Lu1 and Lu2 centers suggest the same origin of these centers, namely that they belong to Lu^{2+} ions, which are perturbed by a defect in a different way.

Despite a much more complex HF structure of Lu2 center, both Lu centers show similarity in angular dependence of their HF structures as one can see from the spectra presented in Fig. 4, where the spectral lines of both centers are visible. Namely, at the majority of magnetic field directions, the HF lines are grouped into two structures related to dominating quadrupole interactions. The HF structure for the Lu2 center is very rich at **B** || b (bottom spectrum in Fig. 4). Moreover, it contains forbidden quadrupole transitions visible well as satellites at 371 and 387 mT.

The quadrupole effects for the Lu2 center must diminish at **B** || c similarly as for Lu1 center. We perform simulation of the Lu2 HF structure at **B** || c for the LPS crystal doped with Ce and annealed in air. This annealing decreases concentration of the Lu1 centers and their contribution to the total spectrum at **B** || c is negligibly small. In this way, we want to check if the largest HF splitting is produced by two Ir isotopes as concluded in Ref. [10]. The result of the simulation is shown in Fig. 5, where the absorption spectrum is used instead of its derivative to distinctly show a big disagreement between the measured and calculated HF structures. In particular, the calculated HF

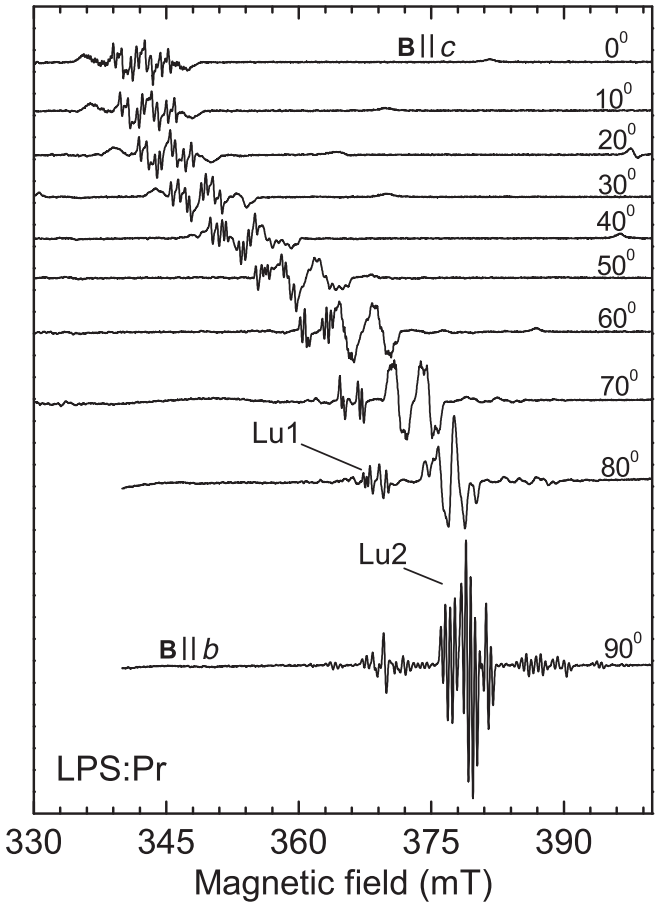

FIG. 4. Angular variation of the Lu2 spectrum in the bc plane. These spectra also contain weak spectral lines from the Lu1 center.

pattern consists of four components of equal intensity since contributions from two Ir isotopes are not distinguished separately. The measured HF structure can be fitted by, at least, six nonequidistant HF components with separation between components much larger than that predicted by the difference in the nuclear g factors of two Ir isotopes. Consequently, this HF structure can hardly belong to Ir isotopes. It is created, as in the case of the Lu1 center, by ^{175}Lu isotope with strong contribution of quadrupole interaction.

2. Trapped hole O^- *center*

As mentioned above, besides electron-type centers, x-ray irradiation also creates a hole-type center. Angular dependencies of resonance fields (center of gravity of HF structure) of this hole center in LPS:Pr (Fig. 6) are fitted by the following g factors: $g_1 = 2.007(1)$, $g_2 = 2.011(1)$, $g_3 = 2.024(1)$, where three principal axes (1, 2, and 3) coincide with the crystallographic axes a*, b, and c. These g-factor values are typical of the O^- hole center usually created by ionizing radiation in oxide materials [16,20–22]. Therefore, it is reasonable to assign this

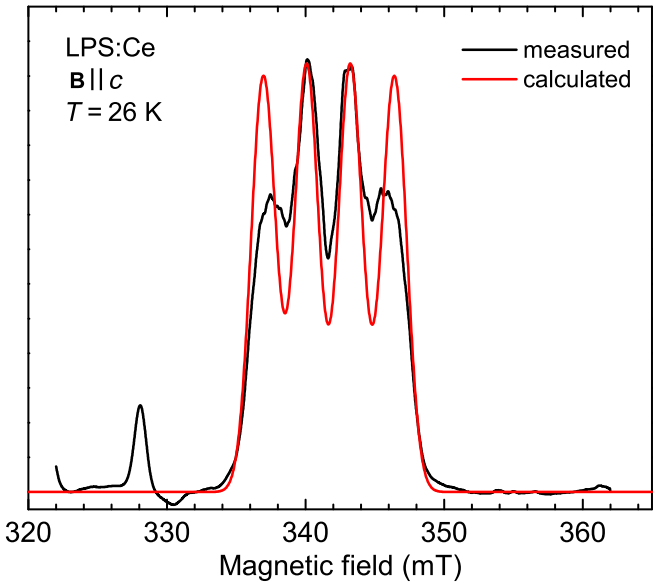

FIG. 5. Simulation of the Lu2 HF structure assuming that only ^{191}Ir and ^{193}Ir isotopes contribute to the HF structure. Dark line presents experimental absorption spectrum; red line is simulated spectrum.

spectrum to a hole trapped at an oxygen ion (O^-, $2p^5$, $S = 1/2$). A similar O^- center is created by x-ray irradiation in LPS:Ce crystal as well. Its spectrum shows approximately the same g factors. However, due to a much broader HF structure (Fig. 7, bottom spectrum) the g-factor actual values are not determined.

The O^- spectrum has a complex HF structure, which can hardly be analyzed. As an example, behavior of the

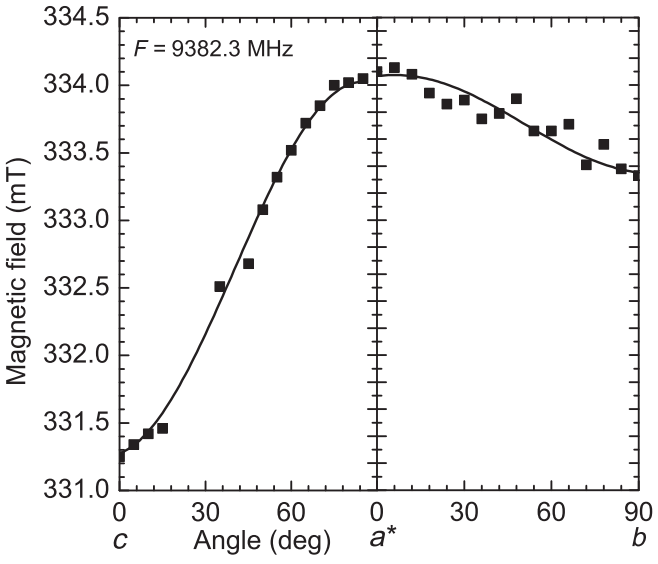

FIG. 6. Angular dependencies of O^- resonance fields (center of gravity of the HF structure) measured for two rotation planes (ca^* and a^*b) in LPS:Pr crystal.

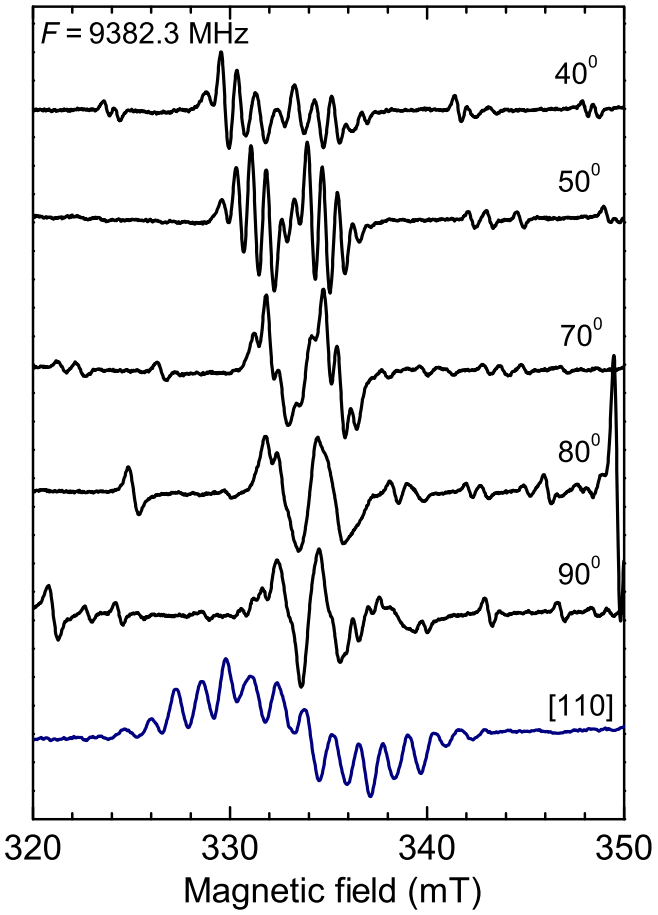

FIG. 7. Angular variation of the O^- center HF structure measured in the ca^* plane of LPS:Pr. The HF structure is poorly resolved at angles <40° as it is overlapped with stronger lines from other centers. The bottom spectrum presents HF structure of the O^- center in LPS:Ce.

HF structure with the angle under rotation of the LPS:Pr crystal in the (ca^*) plane is shown in Fig. 7. One can see, however, that there is a similarity in the HF pattern of this center and those of Lu centers (namely, the HF lines are again grouped into two structures) suggesting that here the unusual HF structure also originates from ^{175}Lu isotopes with strong manifestation of quadrupole effects on HF splitting and appearance of strong forbidden transitions. The lowermost spectrum in Fig. 7 displays the HF structure of the O^- center in LPS:Ce. At this given crystal orientation **B** || [110], the HF pattern contains 15 equidistant lines, which can be attributed to an interaction of the "hole" spin with nuclear spins of two ^{175}Lu isotopes (the number of HF lines is calculated as $n = 2I_{Lu} + 1 = 15$). In the LPS lattice, there are two oxygen ion sites, O2 and O3, which are directly linked to Lu ions in the first neighbor shell. Namely, the O2 ion has two Lu ions, both at the distance of 2.209 Å [17]. Therefore, one can suppose that the hole is located at the O2 ion. Because the HF pattern in

LPS:Pr is almost two times narrower (it contains less spectral lines than that in LPS:Ce) one of the two Lu ions in the O^- center in LPS:Pr is substituted for an impurity ion (or this center includes Lu vacancy) which, as shown below, also increases thermal stability of this center.

B. Temperature stability of the electron and hole centers and comparison with TL

First we check how the high-temperature annealing in air atmosphere influences the centers visible in EPR. Figure 8 compares spectra in LPS:Ce crystal before and after annealing in air at 1400 °C for 6 h. One can see that the high-temperature annealing completely "erases" all the x-ray-created spectra. X-ray irradiation of annealed crystal restores the O^- and Lu2 centers almost with the same EPR intensity, while the Lu1 center is restored with much lower EPR intensity indicating that concentration of these centers substantially decreased after annealing. Such behavior of EPR intensity usually suggests that the center contains an oxygen vacancy (V_O). Trapped electron is thus located at the Lu ion in the vicinity of an oxygen vacancy ($Lu^{2+} - V_O$ center). EPR intensity of the Lu2 center only slightly decreases in annealed crystal suggesting that this center is not related to an oxygen vacancy. Trapped electron at the Lu ion in this center is thus stabilized by another defect. Because the Lu2 center is present only in crystals grown in the Ir crucible [10] one can conclude that this perturbing defect is an Ir^{3+} impurity ion. The corresponding center can be labeled as $Lu^{2+} - Ir^{3+}$ center.

Further experiments are devoted to the determination of thermal stability of the x-ray-induced centers in both the LPS:Pr and LPS:Ce crystals. In this "pulsed annealing" experiment, after x-ray irradiation at room temperature, the sample is heated to a certain temperature T_{ann}, held at that temperature for 5–6 min, and then quickly cooled down to room temperature. Subsequently, the EPR spectrum is measured either at 80–110 K for the O^- center or at 25 K for Lu centers.

Thermal stability data for both crystals are presented in Fig. 9. One can see that the Lu1 center in both crystals is stable at least up to 550 K. In contrast, the O^- center in LPS:Ce shows a lower stability, only up to about 400 K. In LPS:Pr, the O^- center is stable up to about 420 K. In this crystal, thermally liberated holes from oxygen ions recombine at the Lu2 center, markedly decreasing concentration of the Lu2 centers. Lu2 concentration further decreases with the temperature increase. If we compare the data in Fig. 9(a) with TL glow peaks measured in similar LPS:Pr crystals (Fig. 7 of Ref. [9]), one can notice that the position of the main TL peak at 470 K correlates well with the temperature where O^- centers disappear (the TL peak is slightly shifted to higher temperature due to faster heating in TL measurements as compared to our pulsed annealing condition). The high-temperature shoulder in the thermal decay of the Lu2 concentration suggests that electrons are also released at temperatures 450–550 K providing their

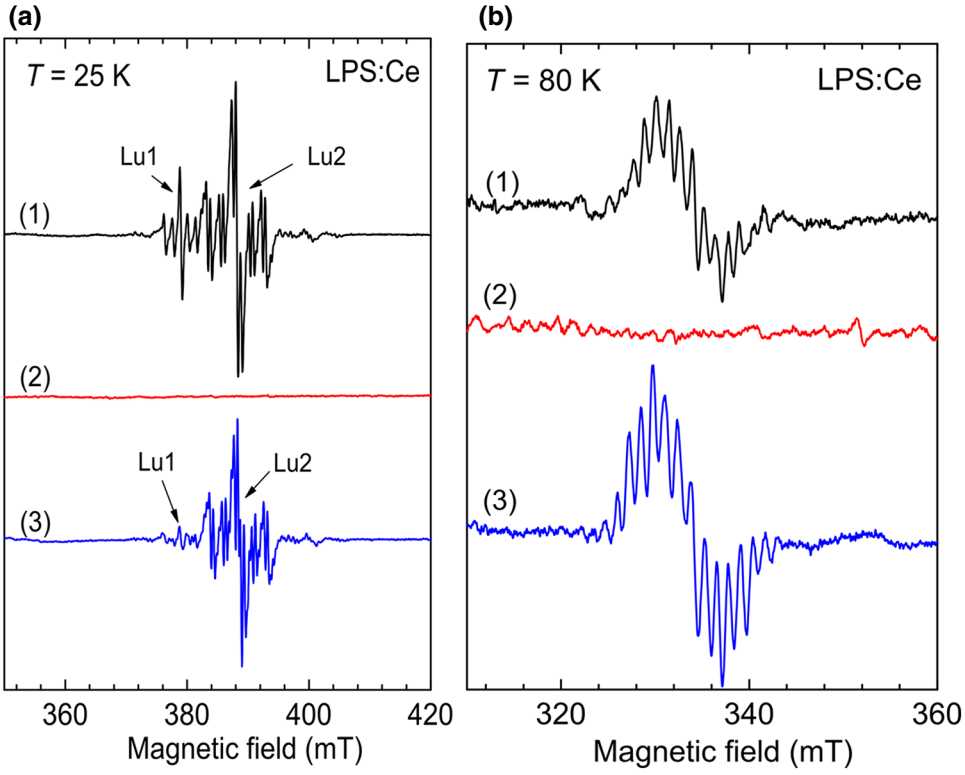

FIG. 8. EPR spectra of the Lu1 and Lu2 centers (a) and O^- center (b) in the LPS:Ce crystal measured in x-ray irradiated "as-grown" crystal (1), in crystal annealed in air at 1400 °C (2), in crystal annealed in air at 1400 °C and then x-ray irradiated (3).

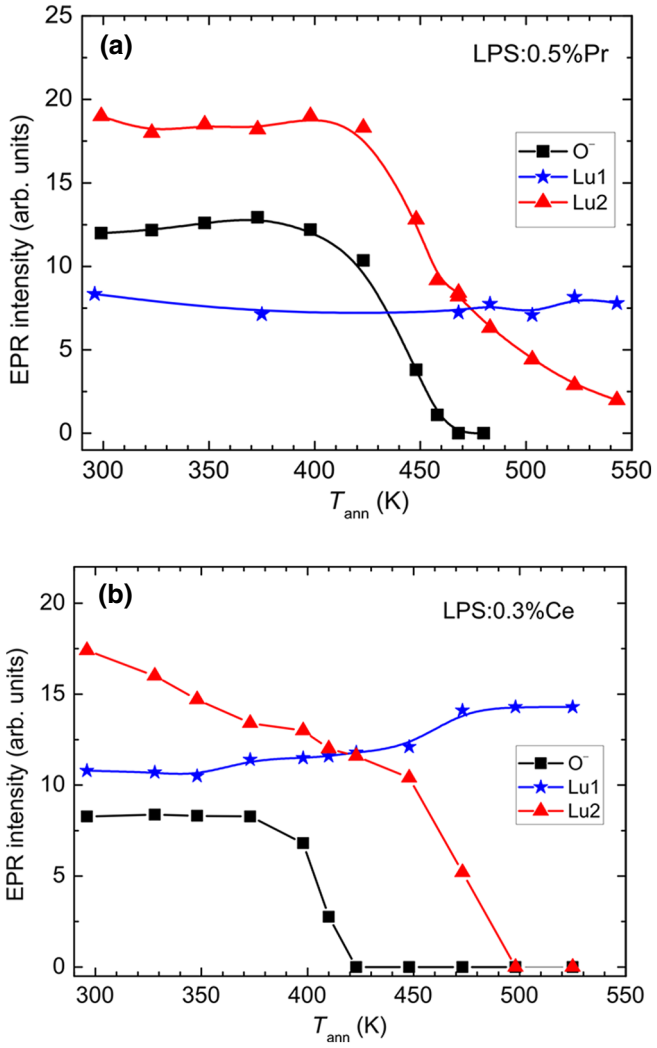

FIG. 9. EPR intensity of the O^-, Lu1, and Lu2 centers (concentration of the ions) as a function of pulsed annealing temperature in the x-ray-irradiated LPS:Pr (a) and LPS:Ce (b) crystal. The EPR intensities presented do not reflect the actual ratio of the ion concentrations.

preferable recombination with holes at Pr^{3+} activator ions. Corresponding high-temperature shoulder is also seen in TL [9].

X-ray-created electron and hole centers in the LPS:Ce crystal show similar temperature intervals of stability. However, their actual behavior with annealing temperature differs from that in LPS:Pr. One can notice that thermal destruction of O^- centers at approximately equal to 400 K does not lead to a visible decrease in the Lu center concentration [Fig. 9(b)]. The TL peak is not seen around this temperature as well [23]. The main TL peak is located at 475 K, where the concentration of Lu2 centers decays. This fact suggests that liberated holes do not recombine at the Lu centers but are rather retrapped by Ce^{3+} ions forming Ce^{4+} states. At a further stage, an electron thermally excited from the Lu2 center recombines with the hole at the Ce^{4+} ion providing the $5d$-$4f$ emission visible in TL. The Lu2 centers also show gradual concentration decrease with increasing temperature. It indicates an electron transfer from Lu2 centers to other defects or impurity ions via tunneling mechanism. This process is so strong that the Lu2 spectrum becomes almost invisible after 2 weeks of the crystal storage at room temperature. First, there is a charge transfer from Lu2 to Lu1 centers since the Lu1 concentration gradually increases with increasing temperature. We also cannot exclude the charge transfer to Ce^{3+} ions. For instance, the tunneling of carries toward rare earth was reported for LPS:Pr crystals [15].

IV. DISCUSSION AND CONCLUDING REMARKS

It should be noted that in previous publications, the Ir^{3+} impurity ions were considered as hole traps in LPS:Ce crystals [10,23]. Our study shows that as in many other oxide materials, namely oxygen lattice ions serve as effective trap sites for holes [20–22]. In contrast, we find that the Ir^{3+} ions serve as a stabilizing defect for electron trapping at the Lu lattice ions. Both the electron and hole trapping phenomena point to polaronic trapping mechanism (bound small polarons [21,22]). The polaronic effect in the LPS lattice is much stronger than that in LSO (YSO) lattice where both the electrons and holes created by irradiation are coupled to lattice ions with much smaller energy. Corresponding O^- and $Y^{2+} - V_O$ (or $Lu^{2+} - V_O$) centers are thermally stable only below room temperature [24]. Similar centers in LPS are stable up to 400–500 K, which is most probably the highest known stability temperature of bound small polaron in oxide materials. Such a large difference in the thermal stability of hole and electron centers in the LPS and LSO lattices is related to the fact that in LSO an electron or hole is trapped at the Si-unbound oxygen ion or vacancy created at this oxygen site. This oxygen ion in LSO is only weakly coupled to the lattice providing a weak bounding energy for the trapped hole or electron [25].

Low-temperature x-ray irradiation of LPS:Pr and LPS:Ce crystals at 77 K creates the same O^- and Lu^{2+} centers similarly to the irradiation at room temperature. Despite the TL glow peaks at 102, 211, and 265 K in both these crystals [9], any additional EPR spectra do not appear at x-ray irradiation at 77 K. This feature indicates that the above-mentioned TL peaks visible below room temperature are created by paramagnetic silent defects.

In many Ce^{3+}- and Pr^{3+}doped scintillation crystals, the 4+ valence state of these activator ions plays an important role in the scintillation mechanism [26–29]. Both these ions can also act as effective hole traps. They store holes before their radiative recombination with electrons. For instance, no O^- hole centers are detected in LSO:Ce crystals [24]. In contrast, in the Ce- and Pr-doped LPS

crystals namely the O^- centers appear after irradiation indicating that primarily holes are trapped at oxygen ions. Only after thermal destruction of the O^- centers the holes can be retrapped at the Ce^{3+} or Pr^{3+} ions or, alternatively, the effective hole trapping by activator ions would be possible only after complete filling of the oxygen ion trapping sites. In that way the oxygen centers would no longer compete with Ce ions in the charge-carrier trapping. This mechanism explains considerable increase of the radioluminescence after prolonged irradiation of LPS crystals [15].

It is difficult to predict if the Ca^{2+} or Mg^{2+} codoping of LPS will have a positive effect on scintillation light yield by stimulating the Ce^{3+} to Ce^{4+} recharge like in LSO [2], since these divalent ions can further stabilize O^- centers. However, a positive effect from the divalent ions codoping could be expected after filling of oxygen trapping sites. Actual concentration of the Ce ions is also a critical aspect in improvement of the LPS scintillation efficiency. This concentration has to be small enough to suppress charge transfer from defect states via tunneling mechanism. At the same time, it has to be large enough to provide an effective energy transfer from the host and the electron-hole radiative recombination at Ce ions.

Note that since with both the Ce and Pr doping in the LPS host there are the same traps and impurities (at least those detectable by EPR) the difference in the light yield in these crystals is hardly related to traps or impurities in the crystals. It is rather an intrinsic property of the Ce^{3+} and Pr^{3+} activator centers and their interplay with the LPS lattice.

Note that according to results of Ref. [10], LPS crystals grown by the floating-zone (FZ) technique demonstrated higher light yield (about 15%) as compared to the crystals grown by the commonly used Czochralski (Cz) method. It could be due to a smaller amount of impurities, like transition metal or rare-earth ions, which enter into the crystal from the crucible during the crystal growth in the case of the Cz-grown materials. In fact, iridium contamination is found in Cz-grown crystals due to the iridium crucible used for crystal growth and scintillation quenching is ascribed to Ir-based traps [10] ($Lu^{2+} - Ir^{3+}$ center). Another possibility is a suppressed number of intrinsic defects, namely oxygen vacancies, which serve as effective traps for electrons ($Lu^2 - V_O$ center), in the FZ-grown crystals. While the atmosphere used in the Cz growth is neutral (argon or nitrogen) or oxygen poor (max. 2% or oxygen can be admixed to neutral atmosphere to prevent burning of iridium crucible), in the case of the FZ growth air atmosphere is usually used. A higher amount of oxygen in atmosphere under crystal growth naturally diminishes the concentration of oxygen vacancies in the crystal. To diminish oxygen-vacancy-based electron traps, the Cz-grown crystals are often annealed in air or oxygen at elevated temperatures [23].

Comparing TL glow curves obtained in LPS crystals grown by the FZ [30] and Cz [6,9,23] methods one may infer that they are quite similar. Both demonstrate complex peaks within the 450–600 K range, two peaks can be distinguished in both cases peaking at approximately 480 and 580 K. There is one more peak at approximately 410 K in FZ-grown crystals [30], whereas it is invisible in the Cz-grown crystal [23]. All this points to rather the same origin of charge-trapping defects in both cases, which depletion is responsible for the 480 and 580 K peaks. Based on this short analysis, one may infer that LPS crystals grown by the FZ and Cz methods contain similar intrinsic defects related to oxygen vacancies, Ir^{3+} ions (when the Ir crucible is used) and O^- ions and thus the results of the present paper can be generalized to cover a wide range of differently grown LPS crystals.

The results obtained in our study can also be applied to all the family of $RE_2Si_2O_7$-based (RE = rare earth) scintillators, namely to the La-admixed $Gd_2Si_2O_7$ (La-GPS) scintillation crystal, which is the derived structure from LPS. Recently it became a prominent topic in scintillation material research due to its high luminescence thermostability, up to 200 °C [31–35] with an excellent scintillation efficiency. It makes La-GPS a serious candidate for applications in environment subject to high temperature (e.g., geophysics, well logging, air and space crafts). EPR in La-GPS is uninformative due to strong exchange coupling of any spin in the lattice with paramagnetic Gd^{3+} host ions. However, similar crystalline and electronic structure of both LPS and La-GPS suggests an existence of similar intrinsic hole and electron traps in these lattices. Thus, the knowledge about the nature of traps in LPS can be used as a guide to optimize also La-GPS because the nature of both electron and hole traps will be closely similar to those in LPS.

ACKNOWLEDGMENTS

The financial supports of the Czech Science Foundation Grant No. 20-12885S and the Ministry of Education, Youth and Sports of Czech Republic, Projects SAFMAT LO1409 and CZ.02.1.01/0.0/16_013/0001406 are gratefully acknowledged.

[1] C. W. E. van Eijk, Inorganic scintillators in medical imaging, Phys. Med. Biol. **47**, R85 (2002).

[2] K. Yang, Ch. L. Melcher, P. D. Rack, and L. A. Eriksson, Effects of calcium codoping on charge traps in LSO:Ce crystals, IEEE Trans. Nucl. Sci. **56**, 2960 (2009).

[3] S. Blahuta, A. Bessière, B. Viana, P. Dorenbos, and V. Ouspenski, Evidence and consequences of Ce in LYSO:Ce,Ca and LYSO:Ce,Mg single crystals for medical imaging applications, IEEE Trans. Nucl. Sci. **60**, 3134 (2013).

[4] Y. Wu, M. Koschan, C. Foster, and Charles L. Melcher, Czochralski growth, optical, scintillation, and defect properties of Cu^{2+} codoped $Lu_2SiO_5:Ce^{3+}$ single crystals, Cryst. Growth Des. **19**, 4081 (2019).

[5] Y. Wu, J. Peng, D. Rutstrom, M. Koschan, C. Foster, and Ch. L. Melcher, Unraveling the critical role of site occupancy of lithium codopants in $Lu_2SiO_5:Ce^{3+}$ single-crystalline scintillators, ACS Appl. Mater. Interfaces **11**, 8194 (2019).

[6] L. Pidol, A. Kahn-Harari, B. Viana, B. Ferrand, P. Dorenbos, J. T. M. de Hass, C. W. E. van Eijk, and E. Virey, Properties of $Lu_2Si_2O_7:Ce^{3+}$, a fast and efficient scintillator crystal, J. Phys.: Condens. Matter **15**, 2091 (2003).

[7] F. He, R. Guohao, W. Yuntao, X. Jun, Y. Qiuhong, X. Jianjun, C. Mitch, and C. Chenlong, Optical and thermoluminescence properties of $Lu_2Si_2O_7$:Pr single crystal, J. Rare Earths **30**, 775 (2012).

[8] P. Dorenbos, Fundamental limitations in the performance of Ce^{3+}, Pr^{3+}, and Eu^{2+}-activated scintillators, IEEE Trans. Nucl. Sci. **57**, 1162 (2010).

[9] E. Mihóková, M. Fasoli, F. Moretti, M. Nikl, V. Jary, G. Ren, and A. Vedda, Defect states in Pr^{3+} doped lutetium pyrosilicate, Opt. Mater. **34**, 872 (2012).

[10] L. Pidol, O. Guillot-Noel, M. Jourdier, A. Kahn-Harari, B. Ferrand, P. Dorenbos, and D. Gourier, Scintillation quenching by Ir^{3+} impurity in cerium doped lutetium pyrosilicate crystals, J. Phys.: Condens. Matter **15**, 7815 (2003).

[11] L. Pidol, B. Viana, A. Kahn-Harari, A. Bessiere, and P. Dorenbos, Luminescence properties and scintillation mechanisms of Ce^{3+}-, Pr^{3+}- and Nd^{3+}-doped lutetium pyrosilicate, Nucl. Instrum. Methods Phys. Res., Sect. A **537**, 125 (2005).

[12] L. Pidol, B. Viana, A. Caltayries, and P. Dorenbos, Energy levels of lanthanide ions in a $Lu_2Si_2O_7$ host, Phys. Rev. B **72**, 125110 (2005).

[13] M. Nikl, A. M. Begnamini, V. Jary, D. Niznansky, and E. Mihokova, Pr^{3+} luminescence center in $Lu_2Si_2O_7$ host, Phys. Status Solidi RRL **3**, 293 (2009).

[14] M. Nikl, G. Ren, D. Ding, E. Mihokova, V. Jary, and H. Feng, Luminescence and scintillation kinetics of the Pr^{3+} doped $Lu_2Si_2O_7$ single crystal, Chem. Phys. Lett. **493**, 72 (2010).

[15] E. Dell'Orto, M. Fasoli, G. Ren, and A. Vedda, Defect-Driven radioluminescence sensitization in scintillators: The case of $Lu_2Si_2O_7$:Pr, J. Phys. Chem. C **117**, 20201 (2013).

[16] M. Nikl, V. V. Laguta, and A. Vedda, Complex oxide scintillators: Material defects and scintillation performance, Phys. Status Solidi B **245**, 1701 (2008).

[17] F. Bretheau-Raynal, M. Lance, and P. Charpin, Crystal data for $Lu_2Si_2O_7$, J. Appl. Cryst. **14**, 349 (1981).

[18] A. Abragam and B. Bleaney, *Electron Paramagnetic Resonance of Transition Ions* (Clarendon Press, Oxford, 1970).

[19] EPR spectra and angular dependencies were simulated using the "Visual EPR" programs by V. Grachev (www.visual-epr.com).

[20] V. V. Laguta and M. Nikl, Electron spin resonance of paramagnetic defects and related charge carrier traps in complex oxide scintillators, Phys. Status Solidi B **250**, 254 (2013).

[21] O. F. Schirmer, O^- bound small polarons in oxide materials, J. Phys.: Condens. Matter **18**, R667 (2006).

[22] V. Laguta, M. Buryi, J. Pejchal, V. Babin, and M. Nikl, Hole Self-Trapping in$Y_3Al_5O_{12}$ and $Lu_3Al_5O_{12}$ Garnet Crystals, Phys. Rev. Appl. **10**, 034058 (2018).

[23] H. Feng, D. Ding, H. Li, Sh. Pan, X. Chen, and G. Ren, Annealing effects on czochralski grown $Lu_2Si_2O_7:Ce^{3+}$ crystals under different atmospheres, J. Appl. Phys. **103**, 083109 (2008).

[24] V. V. Laguta, M. Buryi, J. Rosa *et al.*, Electron and hole traps in yttrium orthosilicate single crystals: The critical role of Si-unbound oxygen, Phys. Rev. B **90**, 064104 (2014).

[25] B. Liu, Z. Qi, M. Gu, X. Liu, S. Huang, and C. Ni, First-principles study of oxygen vacancies in Lu_2SiO_5, J. Phys.: Condens. Matter **19**, 436215 (2007).

[26] M. Nikl, V. Babin, J. Pejchal, V. V. Laguta *et al.*, The stable Ce^{4+} center: A new tool to optimize Ce-doped oxide scintillators, IEEE Trans. Nucl. Sci. **63**, 433 (2016).

[27] Y. Wu, F. Meng, Q. Li, M. Koschan, and Ch. L. Melcher, Role of Ce^{4+} in the Scintillation Mechanism of Codoped $Gd_3Ga_3Al_2O_{12}$: Ce, Phys. Rev. Appl. **2**, 044009 (2014).

[28] F. Moretti, K. Hovhannesyan, M. Derdzyan, G. A. Bizarri, E. D. Bourret, A. G. Petrosyan, and C. Dujardin, Consequences of Ca codoping in $YAlO_3$:Ce single crystals, Chem. Phys. Chem. **18**, 493 (2017).

[29] J. Pejchal, M. Buryi, V. Babin, P. Prusa, A. Beitlerova, J. Barta, L. Havlak, K. Kamada, A. Yoshikawa, V. Laguta, and M. Nikl, Luminescence and scintillation properties of Mg-codoped LuAG:Pr single crystals, J. Lumin. **181**, 277 (2017).

[30] He Feng, Gu Ren, Ji Li, Wu Xu, Qi. Yang, J. Xu, Ji Xu, and Y. Zhang, Energy Transfer and Defects Study in Ce^{3+} and Pr^{3+}, Co-doped Crystal, IEEE Trans. Nucl. Sci 61, 271 (2014).

[31] T. Takasugi, Y. Yokota, T. Horiai, M. Yoshino, A. Yamaji, Y. Ohashi, S. Kurosawa, K. Kamada, V. Babin, and M. Nikl, Al-doping effects on mechanical, optical and scintillation properties of Ce:$(La, Gd)_2Si_2O_7$ single crystals, Opt. Mater. **87**, 11 (2019).

[32] S. Kurosawa, T. Horiai, R. Murakami, Y. Shoji, J. Pejchal, A. Yamaji, S. Kodama, Y. Ohashi, Y. Yokota, K. Kamada, A. Yoshikawa, A. Ohnishi, and M. Kitaura, Comprehensive study on Ce-doped $(Gd, La)_2Si_2O_7$ scintillator, IEEE Trans. Nucl. Sci. **65**, 2136 (2018).

[33] Q. Wei, H. Shi, Z. Zhou, G. Liu, Z. Chen, L. Qin, K. Shu, and Q. Liu, A study on the structure, luminescence and thermos-stability of polycrystalline $Gd_2Si_2O_7$:Ce and $(Gd, La)_2Si_2O_7$:Ce, J. Mat. Chem. C **5**, 1443 (2017).

[34] A. Yoshikawa, Y. Shoji, S. Kurosawa, V. I. Chani, R. Murakami, T. Horiai, K. Kamada, Y. Yokata, Y. Ohashi, and V. Kochurikhin, Czochralski growth of 2 in. Ce-doped $(La, Gd)_2Si_2O_7$ for scintillator application, J. Cryst. Growth **452**, 57 (2016).

[35] A. Yoshikawa, S. Kurosawa, Y. Shoji, V. I. Chani, K. Kamada, Y. Yokata, and Y. Ohashi, Growth, structural consideration, and characterization of Ce-doped $(La, Gd)_2Si_2O_7$ scintillating crystals, Cryst. Growth Des. **15**, 1642 (2015).